ACS Catalysis

Research Article

pubs.acs.org/acscatalysis

Enhanced Hydrogen-Transfer Catalytic Activity of Iridium N-Heterocyclic Carbenes by Covalent Attachment on Carbon Nanotubes

Matías Blanco,[†] Patricia Álvarez,*[,†] Clara Blanco,[†] M. Victoria Jiménez,*[,‡] Javier Fernández-Tornos,[‡] Jesús J. Pérez-Torrente,[‡] Luis A. Oro,[‡] and Rosa Menéndez[†]

[†]Instituto Nacional del Carbón-INCAR, C.S.I.C., 33011-Oviedo, Spain

[‡]Departamento de Química Inorgánica, Instituto de Síntesis Química y Catálisis Homogénea-ISQCH, Universidad de Zaragoza-C.S.I.C., 50009-Zaragoza, Spain

Supporting Information

ABSTRACT: Oxidized multiwall carbon nanotubes (**CNT**) were covalently modified with appropriate hydroxyl-ending imidazolium salts using their carboxylic acid groups. Characterization of the imidazolium-modified samples through typical solid characterization techniques, such as TGA or XPS, allows for the determination of 16 wt % in **CNT-1** and 31 wt % in **CNT-2** as the amount of the imidazolic fragments in the carbon nanotubes. The imidazolium-functionalized materials were used to prepare nanohybrid materials containing iridium N-heterocyclic carbene (NHC)-type organometallic complexes with efficiencies as high as 95%. The nanotube-supported iridium−NHC materials were active in the heterogeneous iridium-catalyzed hydrogen-transfer reduction of cyclohexanone to cyclohexanol with 2-propanol/KOH as hydrogen source. The iridium hybrid materials are more efficient than related homogeneous catalysts based on acetoxy-functionalized Ir−NHC complexes with initial TOFs up to 5550 h^{-1}. A good recyclability of the catalysts, without any loss of activity, and stability in air was observed.

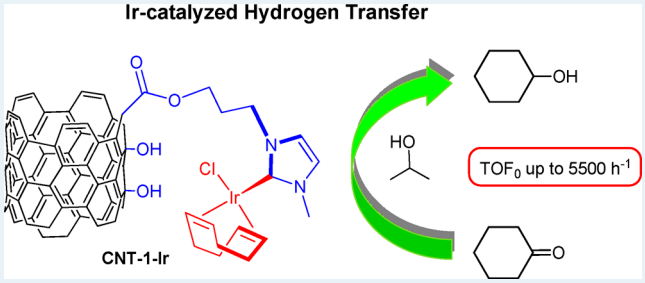

KEYWORDS: *carbon nanotubes, functionalization, iridium, transfer hydrogenation, confinement effect, heterogeneous catalysis*

INTRODUCTION

Carbon-based materials are one of the most versatile matrixes for developing heterogeneous catalysts with enhanced activity.[1] As a particular class within this type of carbon nanostructures, multiwall carbon nanotubes (CNTs) hold a number of inherent properties that make them attractive for catalytic applications. They have, for example, graphite-like walls and an adequate surface area, being more stable toward oxidation (about 650 °C) than activated carbon, and more reactive than graphite. Furthermore, they exhibit an excellent chemical stability (as they are inert in the majority of the reaction media) and also a controlled porosity. A wide range of functional groups can be grafted onto these materials, and in addition, the presence of hollow channels gives rise to new physical properties (e.g., confinement effect).[2] Oxidation is undoubtedly the most common and simplest method to anchor molecular catalysts onto nanotubes and carbon fibers.[3] The oxidation of the nanotubes can be achieved through multiple oxidative agents (air, plasma, electrochemical methods, redox agents, etc.)[4] although it is the use of oxidizing acids, such as nitric and sulphuric acid,[5] which generates a large amount of oxygenated functional groups at the walls (mainly hydroxyl groups) and the tips (mainly carboxylic groups) of the nanotubes without seriously affecting their structure. Thus, by this way it is possible to support platinum, palladium, or gold nanoparticles[6,7] or organometallic complexes, such as the Wilkinson catalyst,[8] on carbon nanotubes. In spite of the successful chemistry of carbon nanotubes with covalent functionalization and the observed mild operating conditions of the catalytic systems based on molecular compounds, there are only a few examples described in the literature.[9]

N-Heterocyclic carbenes (NHC)[10] have recently attracted widespread attention in homogeneous catalysis since they can be used to generate active and stable organometallic complexes.[11] In addition, their tunable character allows for the control of the sterical and electronic properties at the metal center. Additionally, the catalytic activity of the organometallic compounds can be improved by using a carbonaceous support. A good strategy for anchoring NHC ligand precursors on the carbon materials consists of generating ester or amide bonds between the carbon material and the imidazolium ligand using the rich, oxygenated surface chemistry of oxidized carbon nanotubes.[12] In this context, it is worth mentioning that free carbenes have been used as anchor points at CNT side walls.[13]

Received: January 30, 2013
Revised: March 26, 2013
Published: April 30, 2013

   dx.doi.org/10.1021/cs4000798 | ACS Catal. 2013, 3, 1307−1317

The hydrogen transfer process is a good strategy for promoting the reduction of C=O and C=N bonds to generate alcohols or amines under mild conditions that avoids the use of hydrogen gas or other dangerous reducing agents.[14,15] Efficient rhodium and iridium hydrogen transfer catalysts are mainly based both on phosphine and N-donor ligands,[14] although NHC ligands have also been applied to the design of hydrogen transfer catalysts. It has been found that, in contrast to phosphine-based catalysts, iridium−NHC complexes are more active in the reduction of a wide range of unsaturated compounds, such as aldehydes, ketones, or even imines, than their Rh−NHC analogues. Recently, a number of highly efficient iridium−NHC catalysts have been reported.[16] In particular, iridium(I) complexes with hemilabile O- and N-donor functionalized NHC ligands, with methoxy, dimethylamino, and pyridine as donor functions, are efficient catalyst precursors for the transfer hydrogenation of unsaturated compounds in 2-propanol/KOH.[17] However, to the best of our knowledge, there are no reports about the covalent immobilization of iridium complexes on solid supports, in particular, carbon nanotubes, and their application as heterogeneous catalysts in hydrogen transfer. The covalent attachment could improve the activity of the catalysts by permitting the easy recovery and subsequent recyclability of the catalysts.[18]

In this work, the covalent functionalization of oxidized carbon nanotubes with appropriate imidazolium salts is described. To this end, the carboxylic acids were used to form a covalent linkage with the ending OH functional group present in the imidazolium salt. In a second step, the nanotube pendant imidazolium functional groups were employed to generate the corresponding NHC-carbene complexes by reaction with the iridium organometallic compound $[Ir(\mu\text{-}OMe)(cod)]_2$. The catalytic activity of the supported catalysts in the hydrogen transfer reduction of cyclohexanone to cyclohexanol was studied over five consecutive cycles, the last one in air atmosphere in order to determine the reusability and stability of the supported catalyst. Finally, a comparative study with related homogeneous catalysts is also reported.

RESULTS AND DISCUSSION

Characterization of Parent and Functionalized Supports. The carbon nanotubes used in this work were prepared by acid treatment of commercial CVD multiwalled nanotubes (**Raw CNT**), giving rise to the **CNT** sample. According to the TEM observations (Figure 1), the CNTs are 200−600 nm long and exhibit heterogeneous distributions of inner and outer diameters with average values of 6 and 12 nm, respectively. Due to the acid treatment to which the **CNT** samples were subjected, these were free of amorphous carbon and catalyst particles which were confirmed by EDX spectroscopy and TG analysis (see Supporting Information).[19] Both ends of their tips are open, making the inner cavity of the tubes accessible. This was confirmed by the nitrogen adsorption isotherm (see Supporting Information) which evidenced a small hysteresis loop related to the presence of samples with both ends of the tubes open.[20] From these data a mesopore volume content of 0.32 $cm^3\ g^{-1}$ was calculated (V_p, Table 1) with no microporosity detected. The calculated surface BET area (S_{BET}) was 54 $m^2\ g^{-1}$. These data are in accordance with the features expected for acid-treated nanotubes.[20]

The Raman spectra (see Supporting Information) showed an increment of the I_D/I_G ratio after the acid treatment, from

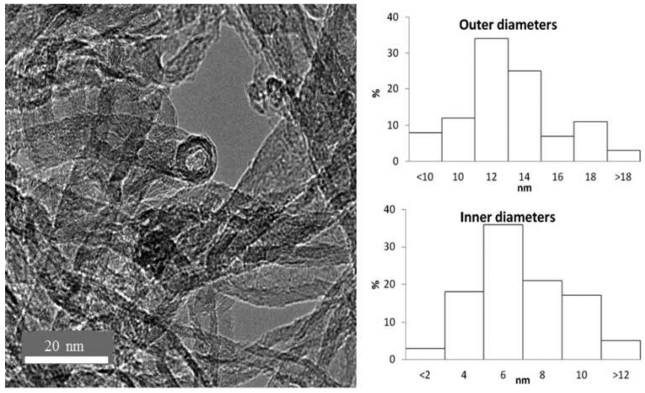

Figure 1. HRTEM image of the oxidized **CNT** with their (inner and outer) diameter distributions.

1.104 in **Raw CNT** to 1.178 in **CNT**, which is consistent with the appearance of defects (i.e., C−O bond formation) during oxidation treatment.

The amount of the functional groups introduced at the walls of the tubes during the acid oxidation can be estimated by means of X-ray photoelectron spectroscopy (XPS). The XPS general spectrum of the **CNT** sample (Table 1) reveals the presence of oxygen at the external surface of the nanotubes in an atomic C/O ratio of 3, which agrees with the oxygen content of oxidized nanotubes reported in the literature.[21] Analysis of the high-resolution C1s peak[22] indicates that the oxygen is mainly in the form of C−O and C=O (7.0 and 3.2%, respectively), with a carboxylic acid group content of 5.4%. Due to steric hindrance, it is to be expected that the acid groups will be located at the edges of the tubes or in defects formed during the acid treatment.[21] Additionally, temperature programmed desorption (TPD) experiments (see Supporting Information) corroborate the presence of oxygenated functional groups in the carbon nanomaterial in the form of 4.68 mmol g^{-1} of desorbed CO_2 and 4.21 mmol g^{-1} of desorbed CO. Deconvolution of the CO_2 and CO curves[23] allowed assignment of 3.81 mmol g^{-1} to carboxylic acid groups.

In order to achieve covalent linkage to organometallic compounds, carbon nanotubes were functionalized with specific imidazolium ligands containing OH-ending groups in the sequence depicted in Scheme 1. As can be seen, the carboxylic groups were initially converted into acid chlorides by reaction with thionyl chloride. These acid chloride groups were subsequently reacted with the imidazolium ligands **1** and **2** through their OH functions. The imidazolium salt, 1-(3-hydroxypropyl)-3-methyl-1*H*-imidazol-3-ium chloride, $[MeImH(CH_2)_3OH]Cl$ (**1**), was synthesized by treating methylimidazole with 3-chloropropan-1-ol as described recently by Doumèche.[24] 1-(2-Hydroxycyclohexyl)-3-methyl-1*H*-imidazol-3-ium iodide, [MeImH(1-cyclohexyl-2-ol)]I (**2**), was synthesized by treating oxabicyclo[4.1.0]heptane with imidazole followed by reaction with methyl iodide in accordance with the procedure of Thiel.[25] Both imidazolium salts were isolated as off-white solids in good yields and fully characterized by NMR.

This two-step procedure gave rise to the functionalized carbon nanotubes **CNT-1** and **CNT-2**. The ^1H NMR in deuterated acetone, where both **CNT-1** and **CNT-2** are slightly soluble, confirmed the successful esterification with the imidazolium salts. The signals corresponding to the imidazolic OH groups were not detected in the spectra, but it was possible

dx.doi.org/10.1021/cs4000798 | ACS Catal. 2013, 3, 1307−1317

Table 1. XPS, Elemental Analysis, Surface Area (S_{BET}), and Volume Pore (Vp) of the Functionalized CNT Samples

sample	C/O[a]	N1s[b]	%N[c]	C sp^2[d] 284.4[e]	C sp^3[d] 284.8[e]	C–O[d] 285.5[e]	C=O[d] 286.5[e]	COOH[d] 288.5[e]	OCOO[d] 290.0[e]	S_{BET}[f]	Vp[g]
Raw-CNT	130			72.8	10.5	8.2	3.9	2.5	1.5	210	2.29
CNT	3	0.4	0.1	64.4	17.1	7.0	3.2	5.4	2.8	54	0.32
CNT-1	6	1.1	1.4	60.3	16.7	9.6	4.5	3.7	5.2	57	0.62
CNT-2	5	1.9	2.1	58.3	16.1	11.9	4.8	2.3	6.9	86	0.69

[a]Carbon/oxygen atomic ratio. [b]Atomic percentage. [c]Determined by elemental analysis. [d]Deconvolution bands of the XPS C1s peak. [e]Data expressed in eV. [f]$m^2\ g^{-1}$. [g]$cm^3\ g^{-1}$.

Scheme 1. Covalent Functionalization of the Parent Carbon Nanotubes with Imidazolium Salts

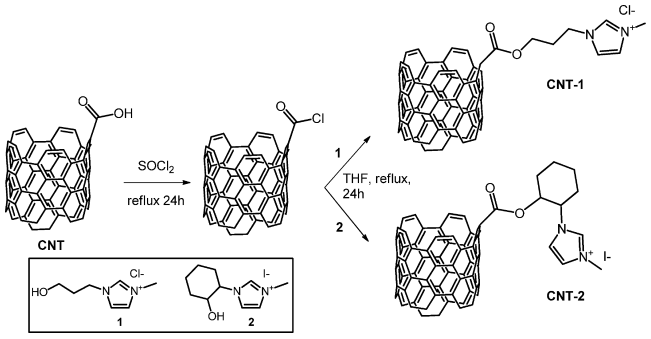

to recognize those corresponding to the imidazolium groups. Particularly, the upfield shifted signals of the characteristic H of imidazolium rings (H2), were observed at δ 8.66 and 8.65 ppm for **CNT-1** and **CNT-2**, respectively. The signals for the olefinic protons in the rings were also observed at δ 7.40 and 7.38 ppm, respectively, with the expected 2:1 ratio compared to imidazolium H (see Supporting Information for details). All these data clearly indicate the linkage of the imidazolium group to the **CNT** material, as was the case for the amide-functionalized carbon nanotubes.[26]

Elemental analysis of the nanotubes indicated an increment in the nitrogen content from 0.1% for the parent CNT to 1.4% for **CNT-1** and 2.1% for **CNT-2**, which is consistent with the linkage of the imidazolium (N-containing) ligand. The higher value obtained in the case of **CNT-2** can be attributed to the presence of a secondary alcohol in **2** which is thermodynamically more reactive toward esterification than the primary alcohol function in **1**. An alternative way of quantification for the amount of linked imidazolium salt is the determination by means of thermogravimetric analysis (TGA, Supporting Information). The weight loss at 400 °C (16 wt % for **CNT-1** and 31 wt % for **CNT-2**) corresponds to the whole imidazolium fragment.[26] An estimation of the molar percentage with respect to the carbon can also be calculated by taking into account the molecular weight of the imidazolium fragment.[27] Thus, the values obtained were 1.03 mol % for **CNT-1** and 1.27 mol % for **CNT-2**, which are also in accordance with the elemental analysis.

By means of XPS (Table 1), an increment in the atomic nitrogen percentage with respect to the parent CNT (from 0.4% in **CNT** up to 1.1% in **CNT-1** and 1.9% in **CNT-2**) was also observed and ascribed to the imidazolic fragments. These results suggest that imidazolium nitrogen atoms in the samples could be located on the external surface of the tubes. However, from a comparison with the elemental analysis data, which are representative of the total amount of nitrogen present in the sample, it is suggested that the increment in the nitrogen content detected by elemental analysis is indicative of the presence of anchored imidazolium salts in the inner cavity of the tubes. Deconvolution of the high-resolution C1s peak (Table 1) of the materials revealed the increase in the binding energy of the C–O band at 285.5 eV, which is attributed to the C–N moieties of the imidazolium ring overlapping this band. Also in support of this argument is the decrease in the COOH peak in favor of functional groups at higher binding energies, which is associated with transformation of the acids into ester moieties due to linkage with the imidazolium ligand.

Finally, TEM observation of **CNT-1** and **CNT-2** samples confirms that the length and diameter of the nanotubes were not modified during the functionalization process (images in the Supporting Information).

Synthesis and Characterization of Iridium Hybrid Catalysts. The deprotonation of the 2-carbon in the imidazolium heterocycle is required for the synthesis of NHC-carbene complexes.[28] In this context, OH-functionalized imidazolium salts have proven to be useful precursors for the

Scheme 2. Synthesis of NHC–Iridium Complexes Anchored on the Carbon Nanotubes

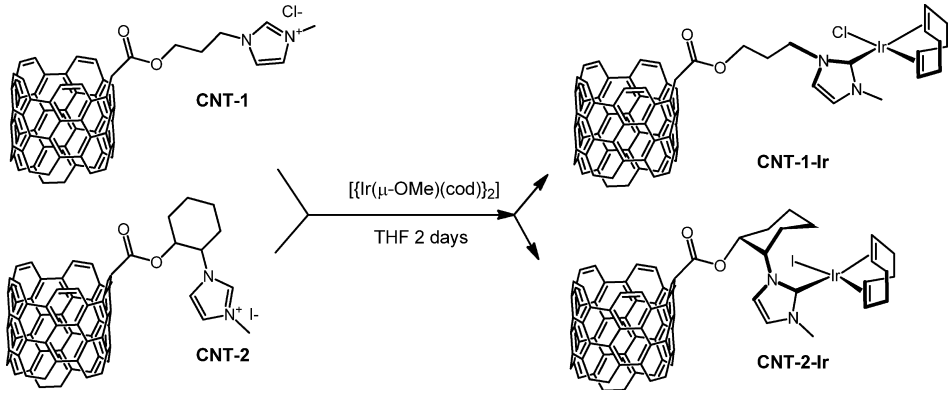

dx.doi.org/10.1021/cs4000798 | ACS Catal. 2013, 3, 1307–1317

preparation of OH-functionalized metal−NHC complexes through well-established synthetic methodologies,[29]

In this way, the imidazolium-functionalized nanotubes samples **CNT-1** and **CNT-2** were reacted with the iridium(I) dimer compound $[Ir(\mu\text{-OMe})(cod)]_2$ (cod =1,5-cyclooctadiene) to produce the hybrid catalysts **CNT-1-Ir** and **CNT-2-Ir** (Scheme 2). The deprotonation of the imidazolium salts linked to the CNTs by the methoxo ligands generated free carbene ligands that were trapped by the metal fragment "Ir(cod)" which completes the coordination sphere with the corresponding counterion (X = Cl, I). Insoluble materials were obtained in both cases, probably as a consequence of the increment in the molecular weight of the samples, which makes them completely insoluble in the reaction media. In fact, these materials were no longer soluble in polar media, which precludes NMR characterization. Although there is no direct evidence, it is thought that the coordination of the iridium complex to the functionalized nanomaterials was achieved through the carbene atom of the heterocycle moiety in a way similar to that of the Ir−NHC homogeneous catalysts. For comparative purposes, the reaction of parent CNT with $[Ir(\mu\text{-OMe})(cod)]_2$ was also studied, which led to the formation of the sample **CNT-Ir** (Scheme 3).

Scheme 3. Possible Anchoring Modes of Ir(I)-cod Fragment through the Carboxylic Groups in CNT-Ir

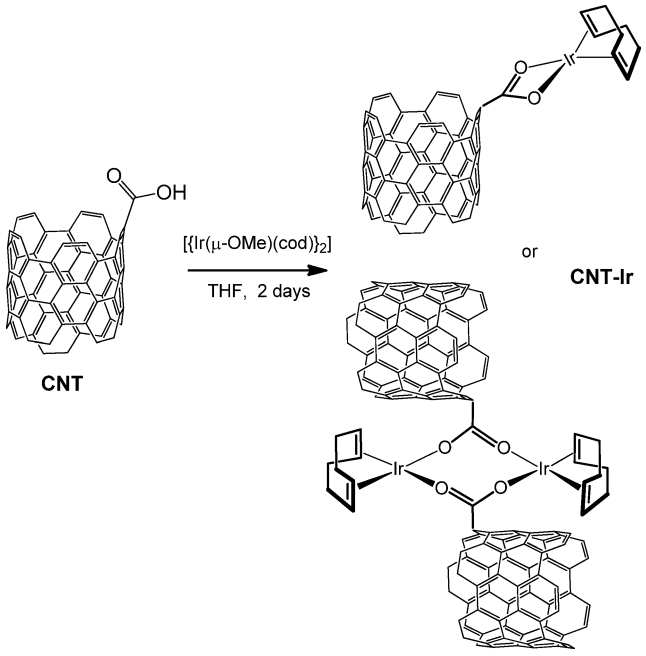

The amount of iridium in the hybrid catalyst was determined by means of ICP-MS measurements. The calculated values were 10.1 wt % for **CNT-1-Ir** and 12.2 wt % for **CNT-2-Ir**. The maximum amount of iridium that can be loaded can also be estimated on the basis of half of the amount of nitrogen introduced into each nanotube sample (two nitrogen atoms per NHC-carbene ring), which are 10.5 and 13.1 wt %, for **CNT-1-Ir** and **CNT-2-Ir**, respectively. From a comparison for the two sets of data it can be concluded that, in both cases, more than 95% of the imidazolium ligands are coordinated to iridium.

The sample without NHC-carbene imidazolium linkers, **CNT-Ir**, gave a 21 wt % iridium. Since the amount of nitrogen both before and after the treatment with the methoxo iridium complex is negligible, it is evident that the attachment of the iridium to the nanotube should be different to that found in samples **CNT-1-Ir** and **CNT-2-Ir**. This was corroborated by an analysis of the Ir4f XPS peak of the three samples (Figure 2).

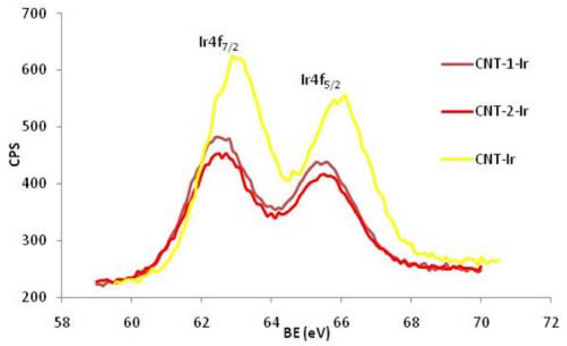

Figure 2. XPS spectra for the Ir4f core level of the hybrid catalysts.

The spectra show two characteristic peaks, the $Ir4f_{7/2}$ peak centered at 62.4 eV and the $Ir4f_{5/2}$ peak centered at 65.6 eV for both **CNT-1-Ir** and **CNT-2-Ir** which are typical of Ir(I) compounds.[30] However, in the sample without NHC linkers, **CNT-Ir**, the maxima is shifted toward higher voltages at 63.0 and 66.1 eV for $Ir4f_{7/2}$ and $Ir4f_{5/2}$, respectively. This fact could be indicative of the presence of iridium in an upper oxidation state as some iridium oxide,[31] but the presence of very different iridium species, as for example iridium nanoparticles,[32] carboxylate-complexes[33] (Scheme 3), or even small di- or triorganometallic clusters,[34] cannot be ruled out. In this context, nickel and iron NPs have been revealed as efficient catalysts for the transfer hydrogenation of ketones.[35] However, to the best of our knowledge, there are no reports on the application of Ir-based NPs in catalytic hydrogen transfer reactions.

Figure 3 shows the HRTEM and HAADF-STEM images obtained for **CNT-1-Ir**. Similar results were obtained for **CNT-2-Ir** (not shown). A first analysis of the samples (and confirmed by EDX, see Supporting Information) reveals the presence of supported iridium catalyst homogeneously distributed at the surface of the nanotubes. Furthermore, some electron-dense regions were detected in the inner cavity of the tubes, which would indicate an inner attachment of the organometallic compound. Iridium species with diameters as low as 0.17−0.27 nm are observed which, according to other authors,[36] could be attributed to the presence of molecular iridium complexes anchored on the surface. The images also show the presence of greater electron-dense regions (1.2−1.4 nm) formed probably as a consequence of the beam damage, which caused migration of the Ir atoms (possibly facilitated by the flexible linkers), formation of iridium clusters, and even subsequent breakup of the resultant clusters into smaller iridium nanoparticles.[37] In fact, electron-dense regions with average sizes of 1.2 nm were also observed when dilute samples of the homogeneous iridium analogues, $[Ir(\mu\text{-OMe})(cod)]_2$ and complex **5** (see below), are evaporated on a carbon grid and then imaged under the same conditions, due to similar electron beam damages (see Supporting Information). These data are in accordance with the XPS data previously described for those materials.

Synthesis and Characterization of Acetoxy-Functionalized Iridium(I)−NHC Complexes. Homogeneous catalysts related to the iridium hybrid materials containing NHC ligands

dx.doi.org/10.1021/cs4000798 | ACS Catal. 2013, 3, 1307−1317

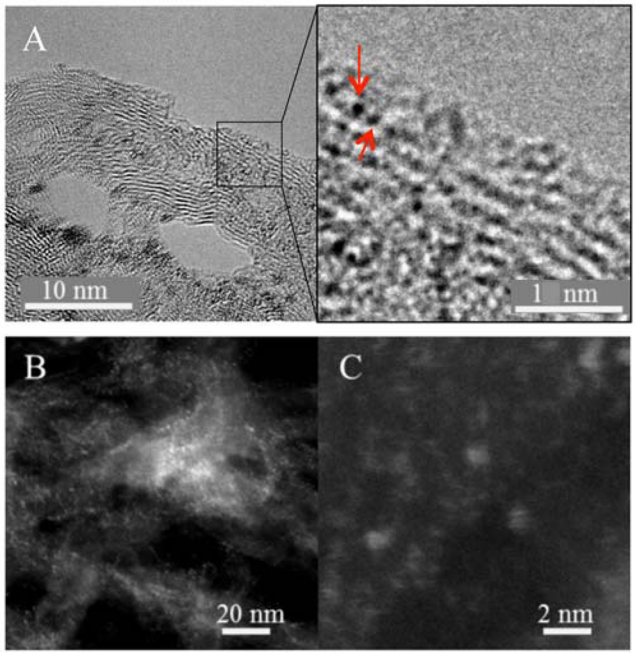

Figure 3. HRTEM (a) and HAADF-STEM (b and c) images of **CNT-1-Ir**.

functionalized with an ester group were synthesized in order to contrast their catalytic activity. Following the general procedures for the preparation of imidazolium salts, 3-(3-acetoxypropyl)-1-methyl-1*H*-imidazol-3-ium chloride, $[MeImH(CH_2)_3OCOCH_3]Cl$ (**3**), was synthesized by reacting methyl imidazole with 3-chloropropylacetate in acetonitrile at 90 °C for 3 days (Scheme 4). The colorless oil obtained was

Scheme 4. Synthesis of the Imidazolium Salt $[MeImH(CH_2)_3OCOCH_3]Cl$ (3)

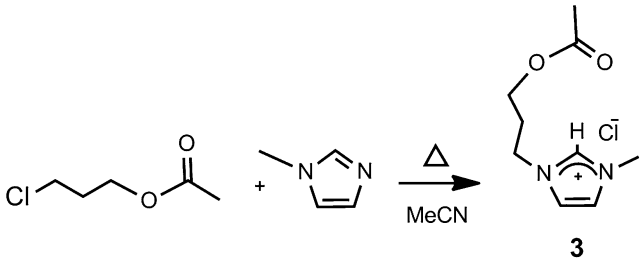

3

characterized by high- resolution mass spectrometry (ESI-HRMS), ^1H and $^{13}C\{^1H\}$ NMR spectroscopy. The characteristic NC*H*N resonance of the imidazolium ring was observed at 9.03 ppm in the ^1H NMR. The acetoxy group was observed at 2.04 ppm in the ^1H and at 172.53 and 20.73 in the $^{13}C\{^1H\}$ NMR spectra.

The imidazolium salt 1-[*trans*-2-acetoxycyclohex-1-yl]-3methyl-1*H*-imidazol-3-ium iodide, [MeImH-(cyclohexylacetate)]I (**4**), was prepared by ring-opening of epoxycyclohexane with imidazole together with acylation to isopropenylacetate followed by alkylation with CH_3I.[25,38]

Complexes $[IrCl(cod)(MeIm(CH_2)_3OCOCH_3]$ (**5**) and $[IrCl(cod)(MeIm(cyclohexyl\text{-}OCOCH_3)]$ (**6**) were prepared from **3** and **4**, respectively, following a two-step procedure. First, the corresponding imidazolium salt was treated with Ag_2O to give a solution of NHC−Ag complex. Then, the concentrated solutions obtained after elimination of the excess of silver oxide were reacted with 0.5 equiv of $[\{Ir(\mu\text{-}Cl)(cod)\}_2]$ dissolved in acetone at room temperature to give the new Ir(I)−NHC complexes which were isolated as yellow solids with good yields (Scheme 5).

Scheme 5. Synthesis of Complexes $[IrCl(cod)(MeIm(CH_2)_3OCOCH_3]$ (5) and $[IrCl(cod)(MeIm\text{-}(cyclohexyl\text{-}OCOCH_3)]$ (6)[a]

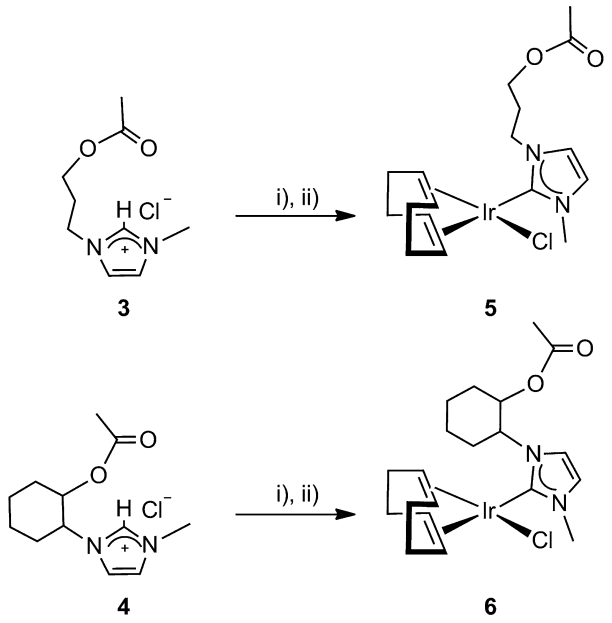

[a]Reagents and conditions: i) Ag_2O, CH_2Cl_2, 48 h, 298 K; ii) 1/2$[\{Ir(\mu\text{-}Cl)cod)\}_2]$ in acetone, 298 K.

Compounds **5** and **6** were characterized by elemental analysis, mass spectrometry (MALDI-TOF), and NMR spectroscopy. The ^1H NMR spectra showed no resonances attributable to the NCHN proton, which confirms the deprotonation of the imidazolium fragment. The coordination of the carbene to the iridium center becomes evident in the $^{13}C\{^1H\}$ NMR spectra which exhibit the characteristic upfield resonance for the carbenic carbon atom at 180.89 ppm (**5**) and 180.64 ppm (**6**). These chemical shifts lie in the usual range for related Ir(I)−NHC complexes.[39] In accordance with the proposed structure, the NMR spectra of the complexes showed four resonances for the =CH olefinic protons of the 1,5-cyclooctadiene ligand, both in the ^1H and in the $^{13}C\{^1H\}$ NMR spectra. This observation is in agreement with the existence of different ligands in *trans* positions and is indicative of the lack of an effective symmetry plane in the molecules probably as a result of the hindered rotation[40] around the carbene−iridium bond due to the effect of substituents in the NHC ligand. On the other hand, the complexes are neutral as was evidenced by the conductivity measurements in acetone which confirm the coordination of the chloro ligand in both complexes.

Catalytic Activity and Recycling. The iridium hybrid catalysts **CNT-1-Ir** and **CNT-2-Ir** and related homogeneous catalysts **5** and **6** were tested as catalyst precursors for the reduction of cyclohexanone to cyclohexanol using 2-propanol as hydrogen source (eq 1, catalytic reaction conditions for transfer hydrogenation of cyclohexanone with 2-propanol). The utilized reaction conditions were those previously optimized for hydrogen transfer processes involving several unsaturated

dx.doi.org/10.1021/cs4000798 | *ACS Catal.* 2013, 3, 1307−1317

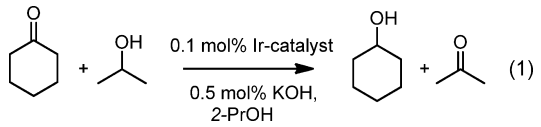

substrates, including cyclohexanone, catalyzed by [IrBr(cod)-(MeIm(2-methoxybenzyl))].[17] Also, 2-propanol was used as hydrogen source because of its nontoxic nature with a moderate boiling point, being at the same time the reaction solvent. Standard catalyst loads of 0.1 mol %, with 0.5 mol % of KOH as cocatalyst, and at 80 °C were routinely employed.

The reaction times required to reach conversions over 90% (as determined by GC using mesitylene as internal standard) and the average turnover frequencies (TOF), calculated at the initial time and at 50% conversion, for all the examined catalysts are shown in Table 2. The results of the tests were compared

Table 2. Catalytic Hydrogen Transfer from 2-Propanol to Cyclohexanone with Iridium Acetoxy-Functionalized Iridium(I)−NHC Complexes and Iridium Hybrid Catalysts[a,b]

entry	catalyst	time (min)	conversion (%)	TON	TOF_0/h^{-1}	TOF_{50}/h^{-1}
1	**5**	210	94	941	4680	2500
2	**6**	270	92	924	2292	1579
3	**7**	220	95	952	3020	2000
4	**CNT-1-Ir**	80	94	943	5550	3750
5	**CNT-2-Ir**	130	93	932	2540	1200
6	**CNT-Ir**	180	10	101	30	–
7	**CNT-2**	180	0	–	–	–

[a]Reaction conditions: catalyst/substrate/KOH ratio of 1/1000/5, $[catalyst]_0 = 1 \times 10^{-3}$ M in 2-propanol at 80 °C. [b]The reactions were monitored by GC using mesitylene as internal standard.

with those obtained from two blank experiments. As the first blank, we used **CNT-Ir** as catalyst which contains no NHC-carbene linker between the carbon material and iridium. As can be observed in Table 2 (entry 6) only 10% conversion was achieved after 3 h of reaction. Thus, catalysts without an Ir−NHC core have a poor balance. The second blank tested was the carbon material **CNT-2**, i.e. CNT functionalized with the imidazolium salt **2** but without iridium. The reaction under these conditions led to 0% conversion after 3 h (Table 2, entry 7). These results illustrate the activity of iridium complexes in hydrogen transfer reactions[14] and, in particular, the outstanding efficiency of the NHC-based iridium catalysts. In addition, the influence of the acetoxy group on the functionalized NHC-carbene iridium complexes **5** and **6** was analyzed by contrasting their catalytic activity to that exhibited by the known complex [Ir(cod)(Me_2Im)I] (**7**) (Me_2Im = 1,3-dimethyl-imidazol-2-ylidene) with an unfunctionalized NHC ligand,[41] synthesized following the Herrmann method.[42]

Both the homogeneous and the supported iridium catalytic systems were found to be active in the transfer hydrogenation of cyclohexanone to cyclohexanol. In general, as can be observed in Table 2 (entries 1−2, and 4−5), heterogeneous catalysts **CNT-1-Ir** and **CNT-2-Ir** were more active than the corresponding homogeneous catalysts **5** and **6** which becomes evident from the required time to reach conversions over 90%. Interestingly, a 94% conversion in only 1.3 h was obtained using **CNT-1-Ir** as catalyst with an average TOF at 50% conversion of 3750 h^{-1}. In both series, the catalysts containing acetoxypropyl-functionalized NHC-carbene ligands were the most active with initial TOFs of 4680 h^{-1} (**5**) and 5550 h^{-1} (**CNT-1-Ir**). In addition, the presence of an acetoxy group has a little effect on the catalytic activity of the homogeneous catalysts, thereby evidencing a limited hemilabile influence. In fact, compound **7**, having an unfunctionalized NHC ligand, exhibited and intermediate catalytic activity compared to that of the acetoxy-functionalized NHC complexes, as it is only slightly more active than **6** but less active than **5** (entry 3).

The enhancement catalytic activity observed with the nanohybrid catalysts could be explained by electronic modifications in the metal center caused by the support or by confinement effects due to the porosity of the material,[2,8,43] especially in the iridium complexes located in the inner cavity of the nanotubes, where the walls of the nanotubes may act as a "nano-reactor". Although the unconjugated linkers in the nanohybrid materials make difficult the electronic communication with the iridium center, the possibility of a surface effect due to the presence of additional functionalities cannot be ruled out (vide infra). The transfer hydrogenation of cyclohexanone was monitored by GC analysis taking 0.1 mL aliquots of the reaction mixture at different time intervals. As can be observed in the conversion vs time plots (Figure 4), no induction period

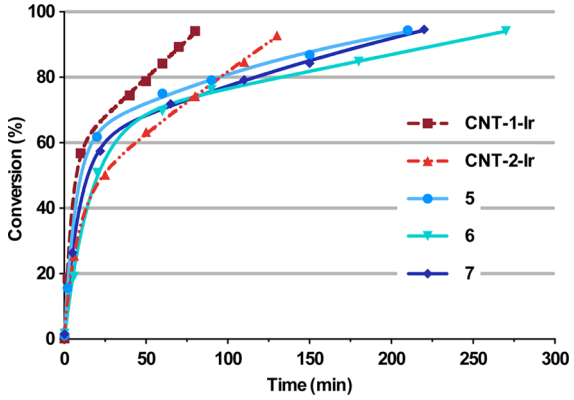

Figure 4. Reaction profiles for transfer hydrogenation of cyclohexanone by homogeneous and heterogeneous catalysts.

was detected, as cyclohexanone reduction was observed immediately after thermal equilibration of the reactant mixture. In general, the kinetic profiles are very similar for all the homogeneous and heterogeneous catalysts. However, the hybrid catalyst **CNT-1-Ir** is the most active species at any time, and even catalyst **CNT-2-Ir** is more active than the homogeneous systems for conversions over 70%. The lower catalytic activity exhibited by **CNT-2-Ir** could be related to steric hindrance caused by the rigid cyclohexylacetate linker to the nanotube walls, making more difficult the access of the cyclohexanone to the active center and also the release of cyclohexanol after reduction.

From the similarities observed between the catalytic reaction profiles, it can be inferred that the reaction mechanism does not change dramatically when the catalyst is supported. Thus, an inner-sphere transfer hydrogenation mechanism with a monohydride complex as active catalytic species can be expected, similar to that proposed for the transfer hydrogenation of unsaturated compounds in 2-propanol/KOH catalyzed by iridium(I) complexes having hemilabile O- and N-donor functionalized NHC ligands.[17] On the basis of this mechanism in homogeneous phase, the closely related

dx.doi.org/10.1021/cs4000798 | ACS Catal. 2013, 3, 1307−1317

mechanism depicted in Scheme 6 is proposed for the hybrid catalysts. The first step is the β-H elimination from the alkoxo

Scheme 6. Proposed Mechanism for the Catalytic Transfer Hydrogenation of Cyclohexanone by the Nanotube-Supported Iridium−NHC Catalysts

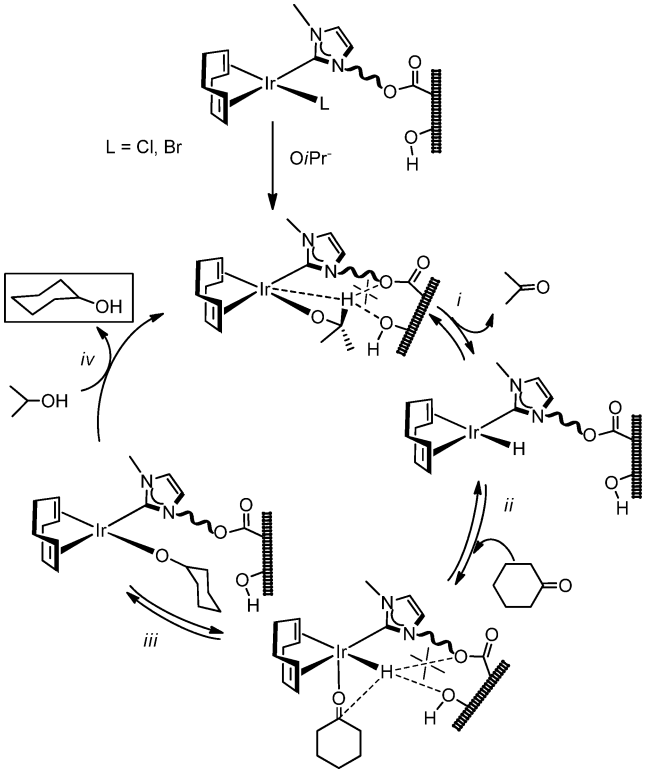

complex [Ir(O*i*Pr)(cod)(NHC-OCO-CNT)] to generate the hydride intermediate [IrH(cod)(NHC-OCO-CNT)] with the concomitant formation of acetone (step i). The coordination of the cyclohexanone substrate to the unsaturated hydride complex (step ii) and the migratory insertion into the Ir−H bond (step iii) result in the formation of a new supported alkoxo complex. Finally, the protonation of the alkoxo ligand by 2-propanol (solvent) results in the formation of cyclohexanol regenerating the starting alkoxo supported complex in an alkoxide exchange reaction (step iv).

We have shown that the presence of a methoxy group on the functionalized NHC ligand in the homogeneous catalyst [Ir($NCCH_3$)(cod)(O-NHC)] (O-NHC = MeIm(2-methoxybenzyl) has an impact on catalytic activity which was associated, through experimental tests combined with DFT calculations, to weak interactions in the forward and backward hydrogen transfer from the hydride intermediate [IrH(cod)(O-NHC)] (hydride migration and β-H transfer).[17] The calculations showed an interaction between the β-H on the alkoxo ligand and the oxygen atom of the methoxy fragment of the NHC ligand, which resulted in a net destabilization of the alkoxo intermediate that facilitates the β-H elimination step in route to the key hydrido intermediate species.

The catalytic performance of catalysts **5** and **6** (having acetoxy-functionalized NHC ligands) that is comparable to that of **7** (with an unfunctionalized NHC ligand) is evidence that the acetoxy linker is not responsible for the superior catalytic activity of the supported catalysts. Thus, the enhanced catalytic activity observed for nanotube-supported iridium−NHC catalysts could be related to the influence of additional functionalities on the support. In this case, the −OH groups remaining on the nanotube walls could play the role of the methoxy function in the homogeneous systems, assisting for the key H-transfer involved both in the hydride migration and β-H transfer steps (Scheme 6). In this context, the flexibility of the linker should have an important effect, which is in agreement with the superior catalytic performance of **CNT-1-Ir**.

Recycling studies were carried out with both nanotube-supported iridium−NHC catalysts. The black solids obtained after the catalysis were simply filtered and washed with fresh 2-propanol (4 × 5 mL) and then subjected to another catalytic cycle by addition of further cyclohexanone/KOH/i-PrOH. Interestingly, both supported catalysts exhibited catalytic activity the same as that of the fresh catalysts after four consecutive cycles under an argon atmosphere (Table 3, with comparable conversions after similar times and identical reaction profiles (Figure 5). Furthermore, in sharp contrast

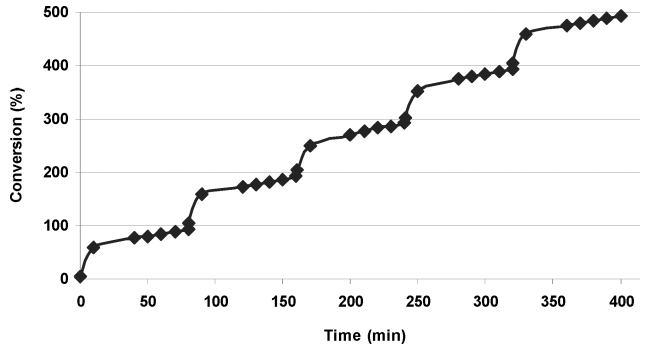

Figure 5. Time dependence of the transfer hydrogenation of cyclohexanone catalyzed by **CNT-1-Ir** in five consecutive runs. The fifth cycle was performed in air.

with the air-sensitivity of the iridium−NHC-based catalyst, these nanotube-supported catalysts were air stable. As it is shown in Table 3, quantitative conversion of cyclohexanone was also achieved when the catalytic reactions were conducted under an air atmosphere in an additional final fifth cycle. The reproducibility of the results and the recycling performance of the catalyst are illustrated in Figure 5 where the same profile feature was observed for every step, even in the catalytic run performed in air.

Table 3. Catalyst Recyclability and Stability Studies[a]

	CNT-1-Ir					CNT-2-Ir				
run	1	2	3	4	5[a]	1	2	3	4	5[a]
time (min)	80	80	80	90	90	130	130	130	130	130
conversion (%)	96	95	96	94	95	95	94	93	94	96

[a]Cycle performed in air.

dx.doi.org/10.1021/cs4000798 | *ACS Catal.* 2013, 3, 1307−1317

At the end of the catalysis runs, the physical state of our catalysts was examined. The XPS measurements of the postcatalysis samples (Figure 6) gave the same binding energy

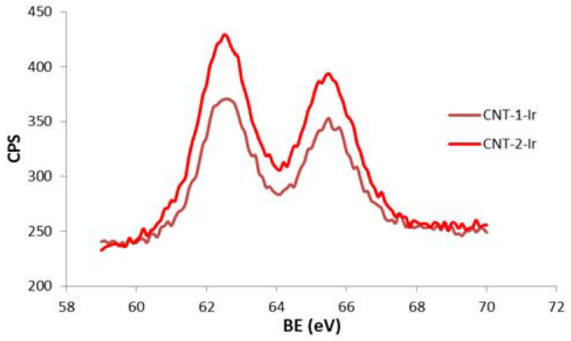

Figure 6. XPS Ir4f region of **CNT-1-Ir** and **CNT-2-Ir** after the catalytic cycles.

values on the $Ir4f_{7/2}$ and $Ir4f_{5/2}$ peaks than before the catalytic cycles. The results clearly suggest that the iridium complexes supported on the carbon nanotubes have not been modified in the hydrogen transfer process. Additionally, HRTEM images of samples **CNT-1-Ir** and **CNT-2-Ir** after the hydrogen transfer cycles (see Supporting Information) exhibit electron dense regions similar to those before the hydrogen transfer cycles.

CONCLUSIONS

We have demonstrated that the ester covalent functionalization of oxidized multiwalled carbon nanotubes with imidazolium salts can be achieved by using the surface carboxylic functional groups generated in the oxidizing acid treatment. The imidazolium-functionalized materials were used to prepare a nanohybrid catalyst containing iridium−NHC-carbene type organometallic complexes with very high efficiencies. The nanotube-supported iridium−NHC materials are efficient heterogeneous hydrogen transfer catalysts for the reduction of cyclohexanone to cyclohexanol using 2-propanol as hydrogen source. Interestingly, the iridium hybrid materials exhibit a more superior performance than related homogeneous catalysts based on acetoxy-functionalized NHC ligands giving almost complete conversions in shorter reaction times. Nevertheless, both types of catalysts present very similar reaction profiles that suggest a similar operating mechanism.

In addition, the heterogeneous catalysts remained stable through successive catalytic runs. This fact confirms that the supported catalyst can be reused in consecutive cycles without any loss of activity, even under an air atmosphere. The confinement effect, due to the porosity of the material, or a surface effect based on the potential cooperation of hydroxyl functional groups on the nanotube walls might explain the notable improvement observed in the catalytic activity.

EXPERIMENTAL SECTION

Scientific Equipment. Characterization of Supports and Hybrid Catalysts. NMR spectra were recorded on a Bruker Advance 300 or a Bruker Advance 400 spectrometer: ^{1}H (300.1276 MHz, 400.1625 MHz) and ^{13}C (75.4792 MHz, 100.6127 MHz). NMR chemical shifts are reported in ppm relative to tetramethylsilane and referenced to partially deuterated solvent resonances. Coupling constants (J) are given in hertz. Spectral assignments were achieved by a combination of $^{1}H-^{1}H$ COSY, ^{13}C APT, and $^{1}H-^{13}C$ HSQC experiments. MALDI-TOF mass spectra were obtained on a Bruker MICROFLEX spectrometer using DCTB (*trans*-2-[3-(4-*tert*-butylphenyl)-2-methyl-2propenylidene]malononitrile) or DIT (Ditranol) as matrixes.[44] Electrospray mass spectra (ESI-MS) were recorded on a Bruker MicroTOF-Q using sodium formiate as reference. Conductivities were measured in $\sim 5 \times 10^{-4}$ M acetone solutions of the complexes using a Philips PW 9501/01 conductimeter. The catalytic reactions were analyzed on an Agilent 4890 D system equipped with an HP-INNOWax capillary column (0.4 μm, 25 m × 0.2 mm i.d.) using mesitylene as internal standard.

Thermogravimetric analyses (TGA) of the materials were performed in a TA SDT 2960 analyzer thermobalance. The procedure was as follow: 5 mg of sample was heated in the thermobalance at 10 °C min^{-1} to 1000 °C using a nitrogen/air flow (1:1) of 200 mL min^{-1}. The molar percentage of imidazole introduced into the carbon nanomaterials can be estimated by quantifying, from the TGA profiles, the weight loss percentage in the range below 400 °C, according to the method described in the literature.[27] Transmission electron microscopy (TEM) was carried out on a JEOL 2000 EX-II instrument operating at 160 kV. High-resolution images of transmission electron microscopy HRTEM and high-angle annular dark-field HAADF-STEM images of the samples were obtained using a JEOL JEM-2100F transmission electron microscope, equipped with a field-emission-gun (FEG) operating at 200 kV. Energy-dispersive X-ray spectroscopy (EDX) was used to verify the atomic composition of the catalyst. The samples were prepared by casting a few drops of 1 mg mL^{-1} ethanol suspensions of the samples over the carbon grids. To minimize exposure of the samples to the air, these were transferred to the lacey carbon grid into a glovebox filled with ultrahigh-purity argon and from the glovebox to the TEM holder to minimize the time required to introduce it into the microscope. The textural characteristics of the samples were analyzed using N_2 adsorption at 77 K. These analyses were performed on ASAP 2020 Micrometrics equipment using around 100 mg of sample in each experiment. Before the experiments, the samples were outgassed at 40 °C for 50 h under vacuum (pressure below 10^{-3} Pa) in order to avoid the desorption of functional groups or damaging the imidazolium salts or the complexes. The apparent surface area (S_{BET}) was determined from the N_2-adsorption isotherm using the BET equation in the range of $P/P°$ between 0.05 and 0.2.[45] The micropore volume was calculated by applying the Dubinin−Radushkevich equation to the N_2 adsorption isotherms,[46] and the total pore volume was obtained from N_2 adsorption when $P/P° = 0.99$. The volume of mesopores was calculated by subtracting the micropore volume from the total pore volume. Elemental analyses were performed on a LECO-CHNS-932 microanalyzer and a LECO-VTF-900 furnace coupled to the microanalyzer. Temperature-programmed desorption (TPD) experiments were performed in a U-shaped quartz cell coupled to a mass spectrometer in order to determine the amount and type of oxygenated functionalities. A sample consisting of 50 mg was heated up to 1000 °C, at a heating rate of 5 °C min^{-1}, under a helium flow rate of 50 mL min^{-1}. The total amount of CO and CO_2 evolved was evaluated in a mass spectrometry analyzer. The X-ray photoemission spectroscopy (XPS) was performed in a SPECS system operating under a pressure of 10^{-7} Pa with a Mg Kα X-ray source. The type of functional groups in the carbon nanotubes was quantified by deconvolution of the high-resolution C1s

dx.doi.org/10.1021/cs4000798 | ACS Catal. 2013, 3, 1307−1317

XPS peak in Gaussian and Lorentzian functions.[47] The amount of iridium present in the samples was determined by means of inductively coupled plasma mass spectrometry (ICP-MS) in an Agilent 7700x instrument; the samples were digested following the method described by Elgrabi et al.;[48] briefly, 30 mg of sample was treated with 5 mL of a mixture of concentrated nitric and hydrochloric acids (3:1 ratio) at 180 °C for 3 h under microwave irradiation.

Raw Materials. The solvents were distilled immediately prior to use from the appropriate drying agents or obtained from a Solvent Purification System (Innovative Technologies). D_2O, $CDCl_3$, and acetone-d_6 were purchased from Euriso-top and used as received. All chemicals, including multiwall carbon nanotubes (MWCNT) were purchased from Aldrich, and reagent grade or better quality was employed in all the experimental work. MeImH (*N*-methyl-imidazole) and cyclohexanone were distilled prior to use.

Raw CVD-grown multiwall carbon nanotubes were oxidized by means of a mixture of sulphuric acid (97%) and nitric acid (60%) in a 3:1 ratio at 80 °C for 20 min, followed by 20 min of ultrasonication. The reaction was quenched with water, and then the mixture was centrifuged for 30 min at 4700 rpm. The supernatant was discarded, and the remaining solid was washed again with water and centrifuged. The process was repeated until neutral pH to give the parent oxidized carbon nanotubes (**CNT**).

The imidazolium salts, $[MeImH(CH_2)_3OH]Cl$ (**1**)[24] and [MeImH(1-cyclohexyl-2-ol)]I (**2**),[25] and the starting organometallic compounds $[\{Ir(\mu\text{-}OMe)(cod)\}_2]$[49] were prepared according to the literature procedures.

Preparation of 3-(3-Acetoxypropyl)-1-methyl-1*H*-imidazol-3-ium Chloride (3). 3-Chloropropylacetate (1.54 mL, 12.5 mmol) was added to a solution of *N*-methylimidazole (1.00 mL, 12.5 mmol) in acetonitrile (15 mL), and the mixture refluxed for 72 h. The colorless oil formed was separated by decantation, washed with *n*-hexane, and dried in vacuum. Yield: 83%. Anal. Calcd for $C_9H_{15}ClN_2O_2$: C, 49.93; H, 6.91; N, 12.81. Found: C, 50.14; H 6.85; N, 12.90. ESI-HRMS (CH_3CN) m/z = 183.11 $[M]^+$. ^1H NMR (298 K, $CDCl_3$): δ 9.03 (s, 1H, NCHN), 7.69 (d, J = 2.0, 1H, CH Im), 7.61 (d, J = 2.0, 1H, CH Im), 4.35 (t, J = 7.1, 2H, NCH_2), 4.14 (t, J = 5.9, 2H, OCH_2), 3.95 (s, 3H, NCH_3), 2.25 (m, 2H, CH_2), 2.04 (s, 3H, $OCCH_3$). $^{13}C\{^1H\}$ NMR (298 K, $CDCl_3$): δ 172.53 (C═O), 136.87 (NCHN), 125.03 (CH Im), 123.76 (CH Im), 61.96 (OCH_2), 47.96 (NCH_2), 36.52 (NCH_3), 30.25 (CH_2), 20.70 (OCH_3).

Preparation of *trans*-2-(1*H*-imidazol-1-yl)cyclohexyl acetate. Synthesized from reaction of isopropenylacetate (6.0 mL, 54 mmol), *trans*-2-(1-imidazolyl)cyclohexanol (1.5 g, 9.0 mmol), and immobilized lipase B from *Candida antarctica* (150 mg, Sigma-Aldrich) in 10 mL of $CHCl_3$. Yield: 56%. ^1H NMR (298 K, CD_3Cl): δ 7.50 (br, 1H, NCHN), 7.03 (t, J = 1.2, 1H, CH Im), 6.93 (t, J = 1.2, 1H, CH Im), 4.88 (m, 1H, NCH), 3.94 (m, 1H, OCH), 2.13 (m, 2H, CH_2), 1.87 (s, 3H, CH_3), 1.84 (m, 2H, CH_2), 1.50−1.35 (m, 4H, CH_2).

Preparation of 1-(2-Acetoxycyclohex-1-yl)-3-methyl-1*H*-imidazol-3-ium Iodide (4). The compound was prepared following a procedure similar to that described by Thiel.[25] Thus, CH_3I (0.307 g, 2.16 mmol) was added to a solution of *trans*-2-(1*H*-imidazol-1-yl)cyclohexyl acetate (0.410 g, 1.97 mmol) in 15 mL of CH_3CN and refluxed overnight. After removing the solvent, the resulting white solid was recrystallized from 2-propanol at 0 °C. Yield: 85%. ^1H NMR (298 K, $CDCl_3$): δ 10.24 (s, 1H, NCHN), 7.38 (t, J = 1.8, 1H, CH Im), 7.33 (t, J = 1.8, 1H, CH Im), 4.95 (m, 1H, NCH), 4.52 (m, 1H, OCH), 4.15 (s, 3H, NCH_3), 2.40 (m, 1H, CH_2), 2.18 (m, 1H, CH_2), 1.98 (s, 3H, CH_3), 1.89 (m, 2H, CH_2), 1.62−1.40 (m, 4H, CH_2).

General Procedure for the Preparation of [IrCl(cod)(MeImROCOCH$_3$)] (R = -(CH$_2$)$_3$- (5); R = -C$_6$H$_{10}$- (6)). The iridium complexes containing acetoxy-functionalized NHC ligands were synthesized through the following two-step procedure. Step 1: A mixture of the imidazolium salts (0.611 mmol) and Ag_2O (0.116 g, 0.5 mmol) were refluxed in dichloromethane (20 mL) for 48 h. The excess of Ag_2O was removed by filtration to give a colorless solution of the NHC−silver complexes. Step 2: Suspensions of $[\{Ir(\mu\text{-}Cl)(cod)\}_2]$ (0.205 g, 0.305 mmol) in acetone (15 mL) were added to concentrated solutions of the previously obtained NHC−silver complexes in CH_2Cl_2 (1 mL). The mixtures were stirred for 24 h at room temperature to give brownish suspensions. The AgX formed was removed by filtration, and the resulting orange solutions obtained were evaporated to dryness under vacuum. The residue was treated with hexane several times to afford the compounds as brownish-yellow solids, which were separated by decantation and dried in vacuum.

[IrCl(cod)(MeIm(CH$_2$)$_3$OCOCH$_3$)] (5). $[MeImH(CH_2)_3OCOCH_3)]Cl$ (0.133 g, 0.611 mmol). Yield: 61%. Anal. Calcd for $C_{17}H_{26}ClN_2O_2Ir$: C, 39.41; H, 5.06; N, 5.41. Found: C, 39.50; H, 5.11; N, 5,53. ^1H NMR (298 K, $CDCl_3$): δ 6.85 (d, J = 2.0, 1H, CH Im), 6.82 (d, J = 2.0, 1H, CH Im), 4.59 (m, 2H CH_2N, 1H CH cod), 4.32 (m, 1H, CH cod), 4.16 (m, 2H, CH_2O), 3.95 (s, 3H, CH_3 Im) 2.98, 2.84 (m, 1H, CH cod), 2.33 (m, 2H, CH_2 cod), 2.21 (m, 2H CH_2, 2H CH_2 cod), 2.10 (s, 3H, OCH_3) 1.81−1.56 (m, 4H, CH_2 cod). $^{13}C\{^1H\}$ RMN (298 K, $CDCl_3$): δ 180.89 (NCN), 171.12 (OCO), 121.94, 120.37 (CH Im), 84.89, 84.60 (CH cod), 61.73 (CH_2N), 51.89, 51.30 (CH cod), 47.55 (CH_2O), 37.48 (CH_3 Im), 34.01, 33.44 (CH_2 cod), 30.38 (CH_2), 30.03, 29.31 (CH_2 cod), 21.10 (OCH_3). MS (MALDI-TOF, DIT matrix, CH_2Cl_2) m/z = 519.4 [M + H], 483.2 [M − Cl]. Λ_M (acetone) = 12 Ω^{-1} cm^2 mol^{-1}.

[IrCl(cod)(MeIm(cyclohexyl)OCOCH$_3$)] (6). $[MeImH(cyclohexyl)OCOCH_3)]I$ (0.213 g, 0.611 mmol). Yield: 55%. Anal. Calcd for $C_{20}H_{30}ClIrN_2O_2$: C, 43.04; H, 5.42; N, 5.02. Found: C, 44.01; H, 5.98; N, 4.89. ^1H RMN (298 K, $CDCl_3$): δ 6.89 (d, J = 2.0, 1H, CH Im), 6.82 (d, J = 2.0, 1H, CH Im), 5.32 (m, 1H, CHO), 5.13 (m, 1H, CHN), 4.61 (br, 2H, CH cod), 3.96 (s, 3H, NCH_3), 3.34 (m, 1H, CH cod), 3.01 (m, 1H, CH cod), 2.25 (m, 4H CH_2, 4H cod), 1.90 (s, 3H, OCH_3), 1.81−1.42 (m, 4H CH_2, 4H cod). $^{13}C\{^1H\}$ RMN (298 K, $CDCl_3$): δ 180.64 (NCN), 170.22 (OCO), 122.17, 119.75 (CH Im), 84.28, 84.00 (CH cod), 73.11 (CHO), 62.77 (CHN), 51.61, 51.67 (CH cod), 37.61 (NCH_3), 33.86, 33.72, 33.56, 32.01 (CH_2), 29.88, 29.66, 24.90, 24.24 (CH_2 cod), 21.07 (OCH_3). MS (MALDI-TOF, DIT matrix, CH_2Cl_2) m/z = 558.3 [M], 523.3 [M − Cl].

Preparation of the Functionalized Nanotubes CNT-1 and CNT-2. The oxidized carbon nanotubes were functionalized with the imidazolium salts following a two-step procedure. First, 0.1 g of oxidized carbon nanotubes (**CNT**) was refluxed in 40 mL of thionyl chloride for 24 h under a nitrogen atmosphere. The resultant product was washed three times with 20 mL of anhydrous tetrahydrofuran (THF) and dried for 2 h under vacuum. Then, the solid was dispersed in 15 mL of anhydrous THF, and 70 mg of imidazolium salt, **1** or **2**,

dx.doi.org/10.1021/cs4000798 | ACS Catal. 2013, 3, 1307−1317

was added under a nitrogen atmosphere. The mixture was refluxed for 24 h. The solid was filtered, and washed with THF (3 × 20 mL), dichloromethane (3 × 20 mL), and ethanol (3 × 20 mL). The solids collected were dried at 100 °C in a preheated furnace. The samples obtained were labeled as **CNT-1** for the imidazolium salt **1** and **CNT-2** for the imidazolium salt **2**.

Preparation of Hybrid Catalysts CNT-1-Ir and CNT-2-Ir. Functionalized carbon nanotubes (with 0.2 mmol of imidazolium salt estimated from the TGA analyses) were mixed with $[Ir(\mu\text{-OMe})(cod)]_2$ (69.6 mg, 0.105 mmol) in 10 mL of THF under an argon atmosphere. The mixture was refluxed for 2 days and then immersed into an ultrasonic bath for 30 min. The resultant solid was recovered by centrifugation, washed with THF (5 × 10 mL) and diethyl ether (2 × 5 mL) and dried under vacuum.

General Procedure for Transfer Hydrogenation Catalysis. The catalytic transfer hydrogenation reactions were carried out under an argon atmosphere in thick glass reaction tubes fitted with a greaseless high-vacuum stopcock. In a typical experiment, the reactor was charged with a solution of cyclohexanone (0.52 mL, 5.0 mmol) in 2-propanol (4.5 mL), internal standard (mesitylene, 70 μL, 0.5 mmol), base (0.1 mL, 0.025 mmol of a KOH solution 0.24 N in 2-propanol) and the catalyst (0.005 mmol, 0.1 mol %). The weight of the supported catalysts used in each catalysis experiment was calculated according to the ICP measurements, assuming that all the iridium in the sample corresponds to active catalyst sites. In that way, 9.51 mg of CNT-1-Ir (10.1 wt % of iridium) and 7.88 mg of CNT-2-Ir (12.2 wt % of iridium) were added. The resulting mixture was stirred at room temperature until complete solution of the catalyst in the case of homogeneous catalyst or 10 min in the case of heterogeneous catalyst and then placed in a thermostatted oil bath at the required temperature, typically 80 °C. Conversions were determined by gas chromatography analysis under the following conditions: column temperature 35 °C (2 min) to 220 °C at 10 °C/min at flow rate of 1 mL/min using ultra pure He as carrier gas.

The material was recovered by centrifugation, once the reaction was completed, and washed with an additional amount of 2-propanol. Several catalytic cycles were performed with this material without adding any fresh catalyst precursor, and in the supported catalysts, at least the last one was carried out without inert atmosphere.

■ ASSOCIATED CONTENT

Supporting Information

Nitrogen adsorption isotherms, Apparent surface area and pore volume, Raman spectra, area ratio for the D and G bands, TPD profiles, TGA curves, TEM and HRTEM images, and ^{1}H NMR data. This material is available free of charge via the Internet at http://pubs.acs.org.

■ AUTHOR INFORMATION

Corresponding Author

*E-mail: par@incar.csic.es (P.Á.), vjimenez@unizar.es (M.V.J.).

Notes

The authors declare no competing financial interest.

■ ACKNOWLEDGMENTS

The authors thank MICINN (Projects Consolider Ingenio 2010 CSD2009-00050 and CTQ 2010-15221) and the Diputación General de Aragón (E07) for their financial support. P.Á. thanks MICINN for her Ramón y Cajal contract. J.F.-T. and M.B. acknowledge their fellowships from MICINN and MECD.

■ REFERENCES

(1) Schaetz, A.; Zeltner, M.; Stark, W. J. *ACS Catal.* **2012**, *2*, 1267−1284.
(2) Pan, X.; Bao, X. *Acc. Chem. Res.* **2011**, *44*, 553−562.
(3) Wildgoose, G. G.; Abiman, P.; Compton, R. G. *J. Mater. Chem.* **2009**, *19*, 4875−4886.
(4) Aqel, A.; Abou El-Nour, K. M. M.; Ammar, R. A. A.; Al-Warthan, A. *Arab. J. Chem.* **2012**, *5*, 1−23.
(5) Osorio, A. G.; Silveira, I. C. L.; Bueno, V. L.; Bergmann, C. P. *Appl. Surf. Sci.* **2008**, *255*, 2485−2489.
(6) Serp, P.; Castillejos, E. *ChemCatChem* **2010**, *2*, 41−47.
(7) Wang, Z.; Zhang, Q.; Kuehnera, D.; Xua, X.; Ivaska, A.; Niu, L. *Carbon* **2008**, *46*, 1687−1692.
(8) (a) Pérez-Cadenas, M.; Lemus-Yegres, L. J.; Román-Martínez, M. C.; Salinas-Martínez de Lecea, C. *Appl. Catal. A* **2011**, *402*, 132−138. (b) Lemus-Yegres, L. J.; Román-Martínez, M. C.; Such-Basáñez, I.; Salinas-Martínez de Lecea, C. *Microporous Mesoporous Mater.* **2008**, *109*, 305−316.
(9) Karousis, N.; Tagmatarchis, N.; Tasis, D. *Chem. Rev.* **2010**, *110*, 5366−5397.
(10) (a) Arduengo, A. J., III; Rasika Dias, H. V.; Harlow, R. L.; Kline, M. *J. Am. Chem. Soc.* **1992**, *114*, 5530−5534. (b) Herrmann, W. A. *Angew. Chem., Int. Ed.* **2002**, *41*, 1290−1309. (c) Bourissou, D.; Guerret, O.; Gabbaï, F. P.; Bertrand, G. *Chem. Rev.* **2000**, *100*, 39−91.
(11) (a) Hahn, F. E.; Jahnke, M. C. *Angew. Chem., Int. Ed.* **2008**, *47*, 3122−3172. (b) Crudden, C. M.; Allen, D. P. *Coord. Chem. Rev.* **2004**, *248*, 2247−2273. (c) Benhamou, L.; Chardon, E.; Lavigne, G.; Bellemin-Laponnaz, S.; César, V. *Chem. Rev.* **2011**, *111*, 2705−2733. (d) Peris, E. *Top. Organomet. Chem.* **2007**, *21*, 83−116.
(12) (a) He, P.; Urban, M. W. *Biomacromolecules* **2005**, *6*, 2455−2457. (b) Wu, Z.; Feng, W.; Feng, Y.; Liu, Q.; Xu, X.; Sekino, T.; Fujii, A.; Ozaki, M. *Carbon* **2007**, *45*, 1212−1218. (c) Deng, X.; Jia, G.; Wang, H.; Sun, H.; Wang, X.; Yang, S.; Wang, T.; Liu, Y. *Carbon* **2007**, *45*, 1419−1424. (d) Malarkey, E. B.; Reyes, R. C.; Zhao, B.; Haddon, R. C.; Parpura, V. *Nano Lett.* **2008**, *8*, 3538−3542. (e) Fagnoni, M.; Profumo, A.; Merli, D.; Dondi, D.; Mustarelli, P.; Quartarone, E. *Adv. Mater.* **2009**, *21*, 1761−1765. (f) Andersson, C.-H.; Grennberg, H. *Eur. J. Org. Chem.* **2009**, 4418−4421.
(13) Lawrence, E. J.; Wildgoose, G. G.; Aldous, L.; Wu, Y. A.; Warner, J. H.; Compton, R. G.; McNaughter, P. D. *Chem. Mater.* **2011**, *23*, 3740−3751.
(14) (a) Gladiali, S.; Alberico, E. *Chem. Soc. Rev.* **2006**, *35*, 226−236. (b) Gladiali, S.; Mestroni, G. Transferhydrogenations. In *Transition Metals for Organic Synthesis: Building Blocks and Fine Chemicals*; Beller, M., Bolm, C., Eds.; Wiley-VCH: Weinheim, Germany, 1998, Vol. 2; pp 97−119.
(15) (a) Guijarro, D.; Oscar, P.; Yus, M. *Tetrahedron Lett.* **2011**, *52*, 789−791. (b) Haraguchi, N.; Tsuru, K.; Arakawa, Y.; Itsuno, S. *Org. Biomol. Chem.* **2009**, *7*, 69−75. (c) Canivet, J.; Süss-Fink, G. *Green Chem.* **2007**, *9*, 391−397. (d) Ikariya, T.; Blacker, A. J. *Acc. Chem. Res.* **2007**, *40*, 1300−1308.
(16) (a) Azua, A.; Mata, J. A.; Peris, E.; Lamaty, F.; Martínez, J.; Colacino, E. *Organometallics* **2012**, *31*, 3911−3919. (b) Gonell, S.; Poyatos, M.; Mata, J. A.; Peris, E. *Organometallics* **2012**, *31*, 5606−5614. (c) Gierz, V.; Urbanaite, A.; Seyboldt, A.; Kunz, D. *Organometallics* **2012**, *31*, 7532−7538. (d) Chiyojima, H.; Sakaguchi, S. *Tetrahedron Lett.* **2011**, *52*, 6788−6791. (e) Newman, P. D.; Cavell, K. J.; Hallett, A. J.; Kariuki, B. M. *Dalton Trans.* **2011**, *40*, 8807−8813. (f) Diez, C.; Nagel, U. *App. Organomet. Chem.* **2010**, *24*, 509−516. (g) Pontes da Costa, A.; Viciano, M.; Sanaú, M.; Merino, S.; Tejeda, J.; Peris, E.; Royo, B. *Organometallics* **2008**, *27*, 1305−1309. (h) Kownacki, I.; Kubicki, M.; Szubert, K.; Marciniec, B. *J. Organomet. Chem.* **2008**, *693*, 321−328. (i) Hahn, F. E.; Holtgrewe, C.; Pape, T.; Martin,

M.; Sola, E.; Oro, L. A. *Organometallics* **2005**, *24*, 2203−2209. (j) Mas-Marzá, E.; Poyatos, M.; Sanaú, M.; Peris, E. *Organometallics* **2004**, *23*, 323−325. (k) Albrecht, M.; Crabtree, R. H.; Mata, J. A.; Peris, E. *Chem. Commun.* **2002**, 32−33. (l) Hillier, A. C.; Lee, H. M.; Stevens, E. D.; Nolan, S. P. *Organometallics* **2001**, *20*, 4246−4252.
(17) Jiménez, M. V.; Fernández-Tornos, J.; Pérez-Torrente, J. J.; Modrego, F. J.; Winterle, S.; Cunchillos, C.; Lahoz, F. J.; Oro, L. A. *Organometallics* **2011**, *30*, 5493−5508.
(18) Shaterian, H. R.; Yarahmadi, H.; Ghashang, M. *Tetrahedron* **2008**, *64*, 1263−1269.
(19) Avilés, F.; Cauich-Rodríguez, J. V.; Moo-Tah, L.; May-Pat, A.; Vargas-Coronado, R. *Carbon* **2009**, *47*, 2970−2975.
(20) Lu, C.; Su, F.; Hu, S. *Appl. Surf. Sci.* **2008**, *254*, 7035−7041.
(21) Datsyuk, V.; Kalyva, M.; Papagelis, K.; Parthenios, J.; Tasis, D.; Siokou, A.; Kallitsis, I.; Galiotis, C. *Carbon* **2008**, *46*, 833−840.
(22) Chiang, Y. C.; Lin, W. H.; Chang, Y. C. *Appl. Surf. Sci.* **2011**, *257*, 2401−2410.
(23) Figueiredo, J. L; Pereira, M. F. R.; Freitas, M. M. A.; Órfão, J. M. M. *Ind. Eng. Chem. Res.* **2007**, *46*, 4110−4115.
(24) Bekhouche, M.; Blum, L. J.; Doumèche, B. *ChemCatChem* **2011**, *3*, 875−882.
(25) Glas, H.; Herdtweck, E.; Spiegler, M.; Pleier, A. K.; Thiel, W. R. *J. Organomet. Chem.* **2001**, *626*, 100−105.
(26) Park, M. J.; Lee, J. K.; Lee, B. S.; Lee, Y. W.; Choi, I. S.; Lee, S. *Chem. Mater.* **2006**, *18*, 1546−1551.
(27) Baskaran, D.; Mays, J. W.; Bratcher, M. S. *Angew. Chem., Int. Ed.* **2004**, *43*, 2138−2142.
(28) Herrmann, W. A. *Angew. Chem.* **2002**, *114*, 1342−1363; *Angew. Chem., Int. Ed.* **2002**, *41*, 1290−1309.
(29) (a) Zarka, M. T.; Bortenschlager, M.; Wurst, K.; Nuyken, O.; Weberskirch, R. *Organometallics* **2004**, *23*, 4817−4820. (b) Edworthy, I. S.; Arnold, P. L. *Chem. Soc. Rev.* **2007**, *36*, 1732−1744. (c) Kühl, O. In *Functionalised N-Heterocyclic Carbene Complexes*; John Wiley & Sons: Chichester. UK. 2010; Chapter 4. (d) Eguillor, B.; Esteruelas, M. A.; García-Raboso, J.; Oliván, M.; Oñate, E.; Pastor, I. M.; Peñafiel, I.; Yus, M. *Organometallics* **2011**, *30*, 1658−1667. (e) Kong, Y.; Wen, L.; Song, H.; Xu, S.; Yang, M.; Liu, B.; Wang, B. *Organometallics* **2011**, *30*, 153−159. (f) Benitez, M.; Mas-Marza, E.; Mata, J. A.; Peris, E. *Chem.—Eur. J.* **2011**, *17*, 10453−10461.
(30) Crotti, C.; Farnetti, E.; Filipuzzi, S.; Stener, M.; Zangrando, E.; Moras, P. *Dalton Trans.* **2007**, 133−142.
(31) Lee, W. H.; Kim, H. *Catal. Commun.* **2011**, *12*, 408−411.
(32) Zahmakiran, M. *Dalton Trans.* **2012**, *41*, 12690−12696.
(33) (a) Díaz-Auñón, J. A.; Román-Martínez, M. C.; Salinas-Martínez de Lecea, C. *J. Mol. Cat. A: Chem.* **2001**, *170*, 81−93. (b) Giordano, R.; Serp, P.; Kalck, P.; Kihn, Y.; Schreiber, J.; Marhic, C.; Duvail, J.-L. *Eur. J. Inorg. Chem.* **2003**, 610−617.
(34) Fritsch, A.; Légaré, P. *Surf. Sci.* **1984**, *145*, L517−L523.
(35) (a) Gawande, M. B.; Guo, H.; Rathi, A. K.; Branco, P. S.; Chen, Y.; Varmad, R. S.; Peng, D.-L. *RSC Adv.* **2013**, *3*, 1050−1054. (b) Sonnenberg, J. F.; Coombs, N.; Dube, P. A.; Morris, R. H. *J. Am. Chem. Soc.* **2012**, *134*, 5893−5899. (c) Alonso, F.; Riente, P.; Yus, M. *Acc. Chem. Res.* **2011**, *44*, 379−391.
(36) Lu, J.; Serna, P.; Aydin, C.; Browning, N. D.; Gates, B. C. *J. Am. Chem. Soc.* **2011**, *133*, 16186−16195.
(37) Uzun, A.; Ortalan, V.; Browning, N. D.; Gates, B. C. *J. Catal.* **2010**, *269*, 318−328.
(38) Barz, M.; Glas, H.; Thiel, W. R. *Synthesis* **1998**, 1269−1273.
(39) (a) Vicent, C.; Viciano, M.; Mas-Marza, E.; Sanaú, M.; Peris, E. *Organometallics* **2006**, *25*, 3713−3720. (b) Mas-Marza, E.; Sanaú, M.; Peris, E. *Organometallics* **2006**, *25*, 3063−3069. (c) Poyatos, M.; Maisse-François, A.; Bellermin-Laponnaz, S.; Gade, L. H. *Organometallics* **2006**, *25*, 2634−2641. (d) Poyatos, M.; Mas-Marza, E.; Mata, J. A.; Sanaú, M.; Peris, E. *Eur. J. Inorg. Chem.* **2006**, 158−162. (e) Field, L. D.; Messerle, B. A.; Vuong, K. Q.; Turner, P. *Organometallics* **2005**, *24*, 4241−4250. (f) Zeng, J. Y.; Hsieh, M. H.; Lee, H. M. *J. Organomet. Chem.* **2005**, *690*, 5662−5671. (g) Mas-Marza, E.; Sanaú, M.; Peris, E. *Inorg. Chem.* **2005**, *44*, 9961−9967. (h) Poyatos, M.; Mas-Marza, E.; Mata, J. A.; Sanaú, M.; Peris, E. *Eur. J. Inorg. Chem.* **2003**, 1215−1221.
(40) Enders, D.; Gielen, H. *J. Organomet. Chem.* **2001**, *617*−*618*, 70−80.
(41) Vázquez-Serrano, L. D.; Owens, B. T.; Buriak, J. M. *Chem. Commun.* **2002**, 2518−2519.
(42) Köcher, C.; Herrmann, W. A. *J. Organomet. Chem.* **1997**, *532*, 261−265.
(43) Malek Abbaslou, R. M.; Soltan, J.; Dalai, A. K. *Appl. Catal., A* **2010**, *379*, 129−134.
(44) Ulmer, L.; Mattay, J.; Torres-García, H. G.; Luftmann, H. *Eur. J. Mass Spectrom.* **2000**, *6*, 49−52.
(45) Brunauer, S.; Emmett, P. H.; Teller, E. J. *J. Am. Chem. Soc.* **1938**, *60*, 309−319.
(46) Dubinin, M. M. *Progress in Surface and Membrane Science*; Academic Press: London, 1975; Vol. *9*.
(47) Sherwood, P. M. A. In *Practical Surface Analysis in Auger and X-ray Photoelectron Spectroscopy*, Briggs, D., Seah, M. P., Eds.; Wiley: New York, 1990; Vol. *1*, p 574.
(48) Elgrabli, D.; Floriani, M.; Abella-Gallar, S.; Meunier, L.; Gamez, C.; Delalain, P.; Rogerieux, F.; Boczkowski, J.; Lacroix, G. *Part. Fibre Toxicol.* **2008**, *5*, 20−33.
(49) Usón, R.; Oro, L. A.; Cabeza, J. A. *Inorg. Synth.* **1985**, *23*, 126−127.